www.czasopisma.pan.pl PAN www.journals.pan.pl

ARCHIVES of FOUNDRY ENGINEERING

ISSN (2299-2944)
Volume 2023
Issue 4/2023

72 – 86

10.24425/afe.2023.146681

9/4

Published quarterly as the organ of the Foundry Commission of the Polish Academy of Sciences

Flow Effect on Si Crystals and Mn-Phases in Hypereutectic and Eutectic Al-Si-Mn Alloys

P. Mikołajczak
Poznan University of Technology, Poland
Corresponding author: E-mail address: Piotr.Mikolajczak@put.poznan.pl

Received 20.06.2023; accepted in revised form 23.08.2023; available online 13.12.2023

Abstract

During mold filling and casting solidification, melt flow caused by gravity is present. Otherwise, forced flow may be a method applied for casting properties improvement. The flow effect generated by an electromagnetic field on the growing phases and a whole microstructure in Al-Si-Mn alloys was studied by slow solidification conditions. The hypereutectic and eutectic alloys were chosen to allow independent growth or joint growth of forming: Si crystals, Mn-rich α-$Al_{15}Si_2Mn_4$ phases and Al-Si eutectics. In eutectic alloys, where Mn-phases precipitate as first and only one till solidus temperature, flow decreased number density of pre-eutectic α-$Al_{15}Si_2Mn_4$. In the hypereutectic alloys, where Mn-phases grow in common with Si crystals, forced convection increased the overall dimension, decreased number density of pre-eutectic Mn phases and strengthened the tendency to growth in the outside of the sample. In the alloys, where Si crystals grow as first, stirring reduce number density of Si and moved them into thin layer outside cylindrical sample. Also by joint growth of Si crystals and Mn-phases, in hypereutectic Mn/Si alloy, flow moved Si crystals outside, reduced number density and increased the dimension of crystals. Stirring changed also AlSi eutectic spacing, specific surface S_v of α-Al and secondary dendrite arm spacing λ_2. The results gave insight of what transformation under stirring take place in simple Al-Si-Mn alloys, and helps to understand what modifications in technical alloys may occur, that finally lead to changes in castings microstructure and properties. The possibility to control dimension, number density and position of Mn-phases and Si crystals is completely new and may help by metallurgical processes, continuous casting of billets and in the production of Si for the solar photovoltaic industry.

Keywords: Casting microstructure, Aluminum alloys, Electromagnetic stirring, Solidification, Si crystals, Mn-phases

1. Introduction

Al–Si base alloys are widely used because of minimum energy requirement for recycling, good corrosion resistance, weldability and high strength/weight ratio. In the microstructure occur primary dendritic grains of α-Al with Al-Si eutectics located in the interdendritic regions [1,2]. Depending on the composition, in alloys containing e.g. Mg, Cu, Fe, Mn, Zn, other phases are present. Manganese (Mn) is important, especially in recycled aluminum alloys, where small amounts of iron (Fe) causes precipitation of platelet shaped β-Al_5FeSi phases. Manganese addition was used to transform β needles into phase as Chinese script or α-Al(Mn,Fe)Si, and that's why the morphology and distribution of Mn phases [3] is such important.

In modern foundry, continuously developed are technologies of: mechanical stirring [4], high shear melt conditioning (HSMC) [5], melt conditioning (MC) [6], thixoforming [7,8], semisolid metal processing (SSM) [9] or rheocasting [10,11]. The advantages of the technologies come from a non-dendritic structure [12] leading to special rheological properties [13] and improving the mechanical properties of aluminum alloys [14] and aluminum based composites [15]. Rotating magnetic fields (RMF) in electromagnetic stirring (EMS) technology [16] improves the properties of billets [17] trough flow induced microstructure transformation.

Development of technologies applying intensive mechanical or electromagnetic melt stirring, and presence of Mn in aluminum based alloys, require continuation in study concerning physical processes, occurring microstructure transformation and technological solutions in production of advanced castings.

In order to simplify the studied microstructures, the hypereutectic and eutectic alloys, from high purity components were prepared. In the Al-Si-Mn system (Figure 1), the compositions were chosen to enable separate (independent growth) or in common (joint) growth of occurring phases: α-$Al_{15}Si_2Mn_4$ phases, Si crystals and Al-Si eutectics. In this way, the flow effect was studied: a) on chosen separated precipitates or on b) growing together phases.

The main motivation was to study individual phases modification and the whole microstructures transformation in the subject of forced-flow technologies development [4-7,10-17].

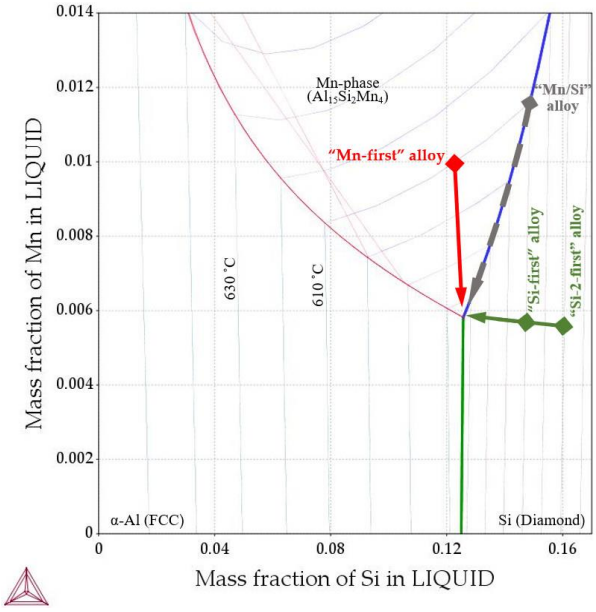

Fig. 1. Ternary Al-Si-Mn phase diagram with for studied alloys marked solidification paths, e.g. dashed gray line for Mn/Si (AlSi14.870Mn1.159) alloy

2. Materials and methods

The hypereutectic and eutectic Al-Si-Mn alloys (Figure 1) were chosen in order to analyze the flow effect on phases growing separately (independent growth) and or in common (joint growth).

The independent growth occurs when only one phase start at liquidus temperature to precipitate (in other words "to solidify"), till the final eutectic reaction. The joint growth occurs when two phases in common at liquidus temperature start to inoculate and grow simultaneously, whilst remaining phases form at solidus temperature. The 610-575 ˚C liquidus-solidus temperature range was chosen and by higher Si content additionally 630-575 ˚C was set. For independent growth were chosen alloys where:

- Mn-rich, α-$Al_{15}Si_2Mn_4$ phase grow first (Figure 1, solid red line) – in alloy called "Mn-first" by precisely calculated composition AlSi12.546Mn1.011,
- Si crystals grow first (Figure 1, solid green line) – in alloy called "Si-first", by precisely calculated composition AlSi14.732Mn0.567, additionally alloy with the composition AlSi16.050Mn0.558 was chosen, called "Si-2-first" (with liquidus temperature 630 ˚C).

For joint, in common growth was chosen one alloy where:

- Si crystals and Mn-rich α-$Al_{15}Si_2Mn_4$ precipitates simultaneously grow (Figure 1, dashed grey line) – in alloy called "Mn/Si", by precisely calculated composition AlSi14.870Mn1.159.

The alloys were prepared in electric furnace with argon degassing and without any modifier, from high purity materials: Mn (99.98% NewMet House, UK), Si (99.9999% NewMet House) and Al (99.999% HMW Hauner GmbH, Germany). After 1.5 h melting at a temperature of 800–805 °C, 38 mm in diameter cylindrical samples with height of 65 mm (Figure 2) were placed in the equipped with electric coils solidification facility [18]. Moved with melt graphite crucibles were insulated Sibral (Unifrax, USA) for low cooling rate and small temperature gradient allowing slow solidification within entire sample, without stirring (RMF 0 mT) leading to equiaxed dendrites, and with electromagnetic field (RMF 11 mT) leading to formation of globular or spherical forms [18-21]. The measured solidification parameters (RMF 0 mT) were: cooling rate $R_{800\text{-}liq}$ = 0.574 (K/s) and temperature gradient $G_{800\text{-}liq}$ = 0.238 (K/mm). The powered electromagnetic coils at 10 A, 45 V and 50 Hz generated flux of 11 mT (Gaussmeter MF100, Extech Instruments, US) [18].

The microsections cut from cylindrical samples (Figure 2) were prepared with standard metallographic procedure including grinding and polishing in Mecatech 250 SPC (Presi, France) and observed with a LOM microscope (Nikon Eclipse MA200, Japan). From 8 experiments 8 cross-sections were analyzed (4 without and 4 with stirring) using ImageJ 1.51a software (Fiji, National Institutes of Health, USA). The microstructure saved at magnifications from 50× to 500×, was analyzed: in one larger area (green dashed line rectangle, Figure 2), in four arch shaped areas (green dashed line) and in four rectangular areas (white-filled) and prepared by the image stitching technique.

The following parameters were determined on the cross-section: number density n_{Mn} and average overall dimension L_{Mn} of manganese-rich α-$Al_{15}Si_2Mn_4$ precipitates, number density n_{Si} and average length L_{Si} of Si crystal, eutectic spacing λ_E for Al–Si eutectics, secondary dendrite arm spacing λ_2 and specific surface S_v of α-Al. In the studied alloys, larger Mn-phases solidifying between liquidus and solidus temperatures were labeled as pre-eutectic Mn phases. Similarly, much smaller Mn-phases precipitating at solidus temperature and being part of ternary eutectics were labeled as inter-eutectic Mn phases. In the measurement of 7699 $Al_{15}Si_2Mn_4$ intermetallics, overall dimension of 2301 pre-eutectic and 5398 inter-eutectic phases were considered, and similarly for Si crystals, leading to calculation of the average overall dimension characterizing occurring phases. For eutectics spacing λ_E, the averaging of the distance between adjacent plates was applied. The averaging of the distance between 10-50 adjacent side branches for determination of secondary dendrite arm spacing λ_2 was applied.

The specific surface S_v of α-Al was determined as the ratio of the perimeter and the enclosed area.

In the current study, author studied phases well-known from 3D X-Ray tomography [3] and many other studies (e.g. in [1,12,13,20-24]): complex shaped $Al_{15}Si_2Mn_4$ phases, Si crystals, dendritic or spherical shaped α-Al and AlSi eutectics. First considered theoretically, the precipitation sequence was next exactly calculated with the Thermo-Calc software [25], used to determine the sequence of phases precipitation, property diagrams, the ternary phase diagram and the Scheil solidification. The calculations gave the exact data of precipitation of only one first phase (e.g. α-$Al_{15}Si_2Mn_4$ in the "Mn-first" alloy) or both (e.g. $Al_{15}Si_2Mn_4$ and Si crystals in "Mn/Si" alloy), with characteristic temperatures and mass fraction of solid phases.

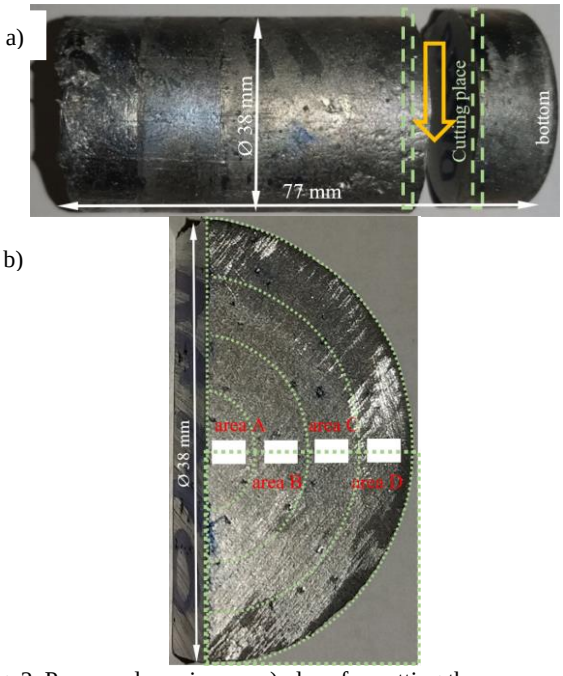

Fig. 2. Processed specimens: a) place for cutting the cross-section, b) areas A, B, C and D for parameters measurement. The dashed green line area used for general observation. The dotted green line show arch shaped area for the measurent of Si crystals, large Mn intermetallics and dendrite arm spacing (magnification 50×). The rectangle shaped white-filled areas were determined for e.g. eutectic spacing measurement (magnification 50× and 200×)

3. Results

The chapter shows flow effect on studied alloys microsections across cylindrical sample and measured parameters characterizing phases. Precipitation sequence with temperatures and mass solid fraction should give insight into microstructure formation.

3.1. Microstructure

Figure 3 presents the microstructure of a Mn-first alloy (AlSi12.546Mn1.011) specimen solidified with and without melt flow, with clearly visible $Al_{15}Si_2Mn_4$ phases distributed across specimen. Higher magnification (Figure 4) shows Mn-phases located in Al-Si eutectics with some small α-Al precipitations occurring shaped as dendrites (white color), inter-eutectic (being part of ternary eutectics) and pre-eutectic Mn phase, and also Al-Si eutectics. Figure 4a presents small inter-eutectic Mn-phases (being part of ternary eutectics) that fit in between Al-Si eutectics, whilst Figure 4b shows larger pre-eutectic Mn-phases that shaped more freely into box [3] similar structures.

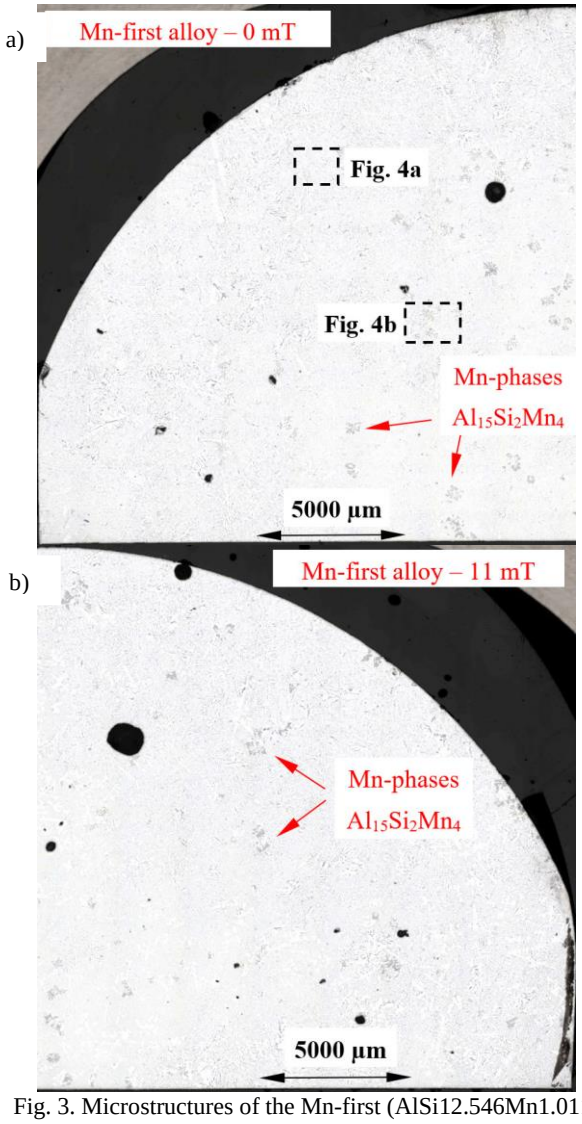

Fig. 3. Microstructures of the Mn-first (AlSi12.546Mn1.011) alloy specimen solidified by flux : (a) 0 mT and (b) 11 mT of electromagnetic field. LOM, magnification 50×

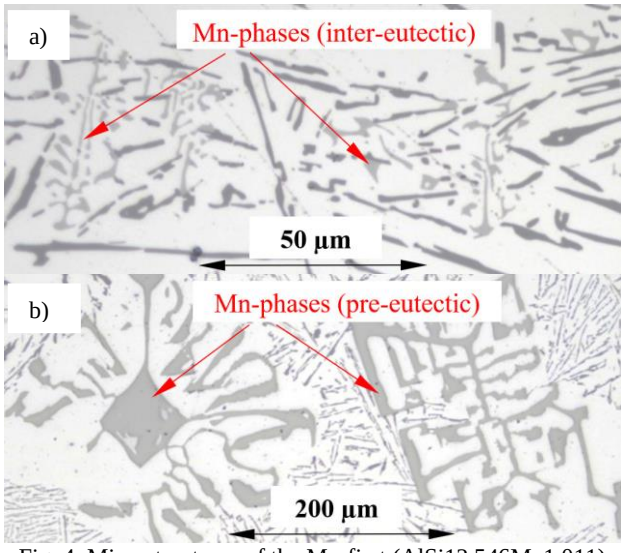

Fig. 4. Microstructures of the Mn-first (AlSi12.546Mn1.011) alloy specimen with: (a) inter-eutectic Mn-phases and (b) pre-eutectic Mn-phases solidified by flux 0 mT of electromagnetic field. LOM, magnification 200×

For Si-first alloy (AlSi14.732Mn0.567) solidified without stirring (Figure 5), it is possible to see the internal area A+B reaching a dimension of 0.5 of radius R (0.5R), filled almost exclusively with Al-Si eutectics, while the external area C+D has many Si crystals (Figure 6). A thinner layer rich in Si formed for solidification with stirring (Figure 5b), in the outside area D, starting from 0.75R to the edge of the specimen, and the amount and dimension of Si crystals seem to be smaller (Figure 5b). By the higher amount of silicon in the Si-2-first alloy (AlSi16.050Mn0.558), the occurrence of the two areas is similar (Figure 7), and the forced flow also changed the dimensions of the areas, starting from radius 0.5R to 0.75R and finishing at sample edge. Fluid flow seems to decrease the amount and location of Si crystals in the Si-first and Si-2-first alloys, forming a thin layer of Si crystals near the outside of cylindrical sample.

On the microstructure (Figure 8) of the Mn/Si alloy (AlSi14.870Mn1.159) there appeared $Al_{15}Si_2Mn_4$ phases, Si crystals, and Al-Si eutectics. Similarly to Si-first and Si-2-first alloys, there formed area rich in Si crystals, that was modified under flow into smaller outside area D. In the case of solidification without stirring, it is possible to see the internal area A+B reaching a dimension of 0.5 of radius R (0.5R), filled almost exclusively with Al-Si eutectics, while the external area C+D has many Si crystals. In the case of solidification with stirring (Figure 8b) formed a thin layer rich in Si, the outside area D is smaller, starting from 0.75R to the edge of the specimen, and the amount and dimension of Si crystals seem to be smaller.

3.2. Parameters characterising microstructure

The effect of electromagnetically generated stirring was characterized by the parameters counted and measured in specified areas (Figure 2) and concerning large number of grains and crystals led to high quality of the results.

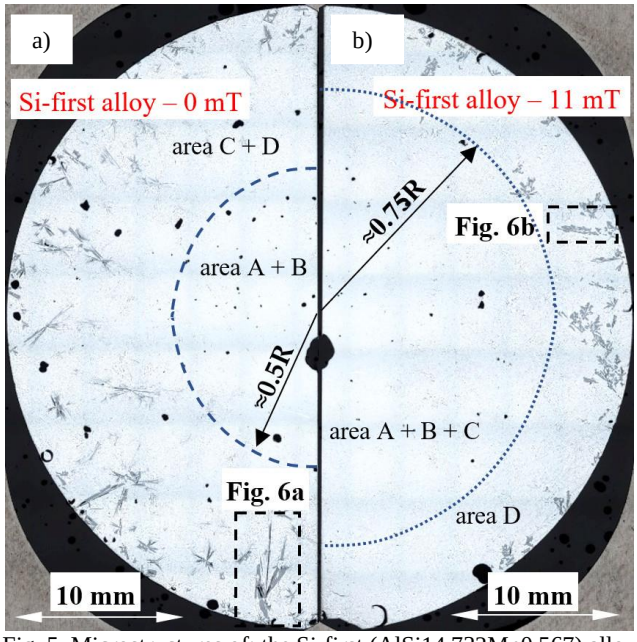

Fig. 5. Microstructures of: the Si-first (AlSi14.732Mn0.567) alloy specimen solidified by flux: (a) 0 mT and (b) 11 mT of electromagnetic field. LOM, magnification 25×

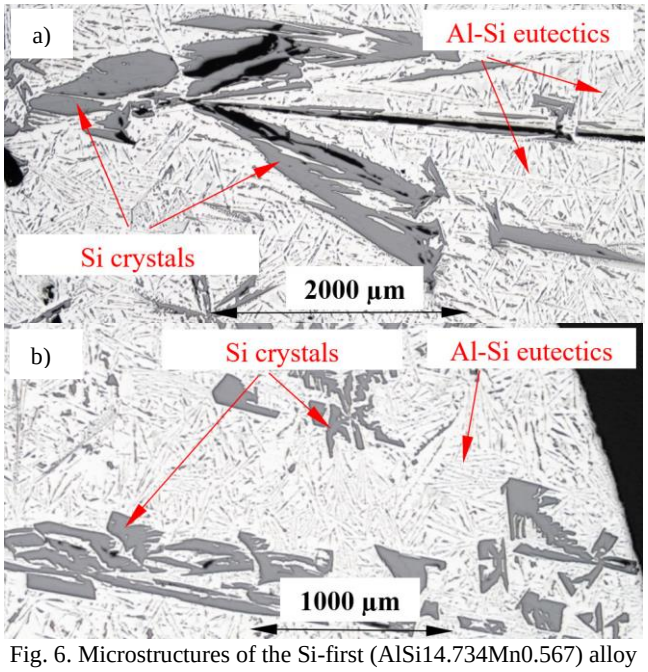

Fig. 6. Microstructures of the Si-first (AlSi14.734Mn0.567) alloy specimen solidified by flux: (a) 0 mT and (b) 11 mT of electromagnetic field. LOM, magnification 100×

In Tables 1-4, the number of inspected phases, crystals grains and dendrite arms is shown in parentheses, whilst the standard deviation is given in square brackets. In Mn-first alloy solidified with flow (Table 1), average overall dimension L_{Mn} amounts 26.94 and was calculated from 248 measured intermetallics and standard deviation amounts σ=1.829 µm. Electromagnetic stirring

caused 44% decrease in L_{Mn} from 47.88 μm to 26.94 μm, increase in solidification time from 464 s to 504 s. Across sample L_{Mn} amounts: 31.51 μm (standard deviation σ=2.01 μm) in area A (Figure 2), 18.54 μm (σ=1.15 μm) in area B, 30.64 μm (σ=2.19 μm) in area C and 35.49 μm (σ=1.50 μm) in area D.

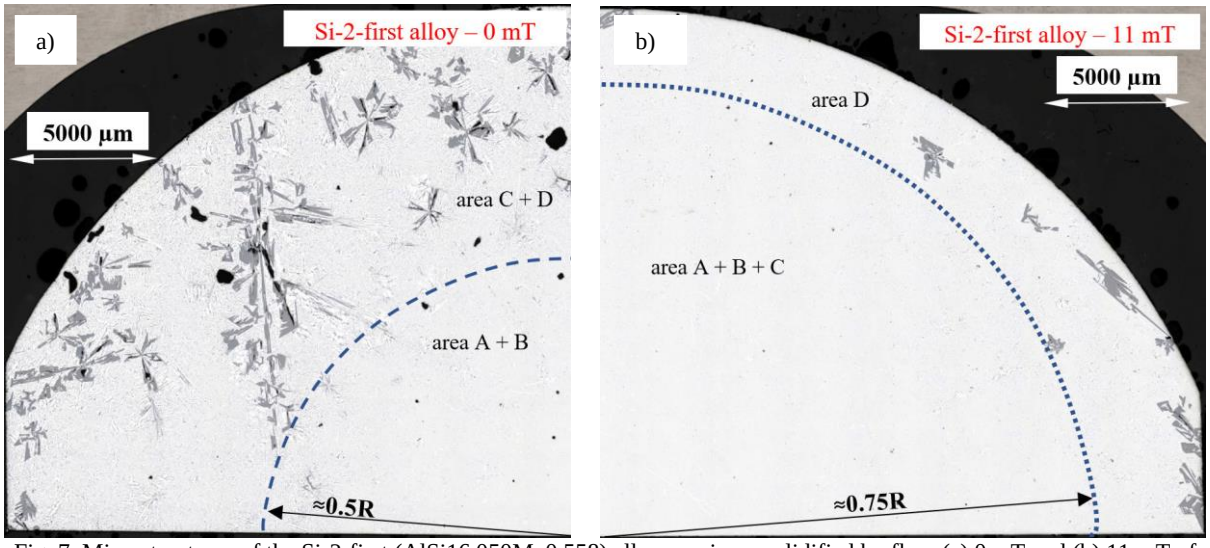

Fig. 7. Microstructures of the Si-2-first (AlSi16.050Mn0.558) alloy specimen solidified by flux: (a) 0 mT and (b) 11 mT of electromagnetic field. LOM, magnification 50×

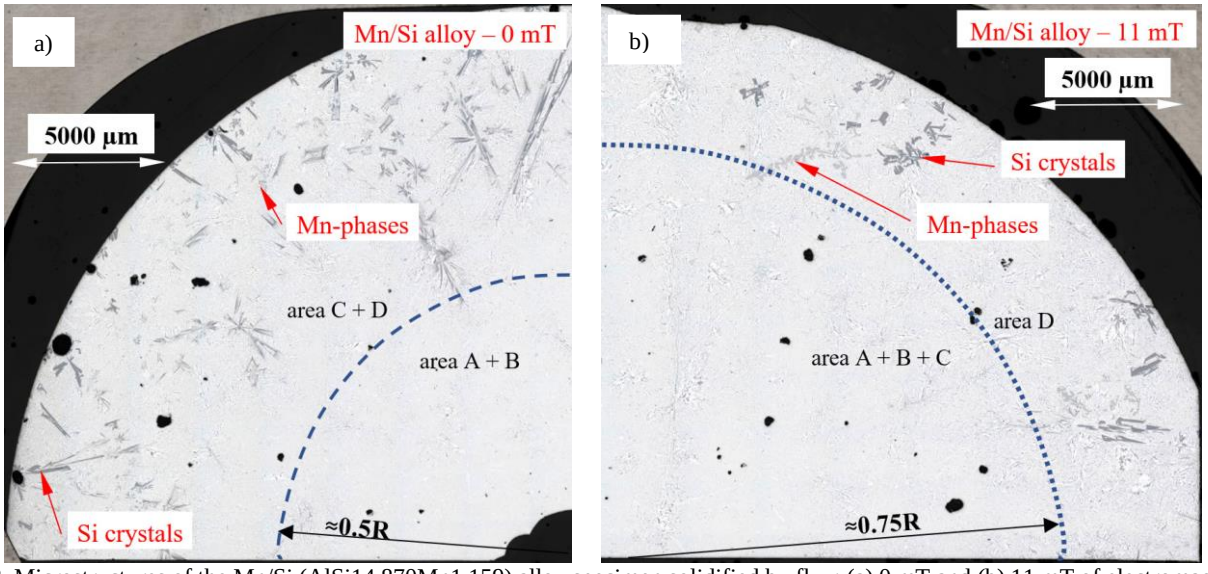

Fig. 8. Microstructures of the Mn/Si (AlSi14.870Mn1.159) alloy specimen solidified by flux: (a) 0 mT and (b) 11 mT of electromagnetic field. LOM, magnification 50×

The average overall dimension L_{Mn} of being part of ternary eutectics inter-eutectic Mn phases (Table 1) decreased by 44% under flow for the Mn-first alloy, from 47.88 μm to 26.94 μm. Similarly for Si-2-first and Mn/Si alloys, L_{Mn} decreased 38% and 47% respectively, whilst it remained unchanged (-4%) for the Si-first alloy (by standard deviation σ=2.221 μm and 2.005 μm). Under forced flow, number density n_{Mn} (Table 2) decreased 30% for Si-first alloy, whilst increased 13%, 25% and 79% for Mn-first, Si-2-first and Mn/Si alloys respectively.

Both decreases and increases were observed for individual alloys and there is no direct modification in the eutectic spacing λ_E (Table 1), and the effect of electromagnetic stirring on (α-Al)-Si eutectic seems unclear. For the Si-first alloy, the eutectic spacing λ_E increased by 21% from 12.65 μm to 15.32 μm, with standard deviation values of 2.51 μm and 2.10 μm, whilst for Mn-first alloy remained unchanged.

For inter-eutectic Mn-phases (being part of ternary eutectics, Table 2), smaller values of average overall dimension L_{Mn} were observed, where the sizes reached 9.98-47.88 μm, in opposite to

pre-eutectic precipitates 382-616 μm. Electromagnetically generated flow caused 61% larger average overall dimension of Mn-phases in Mn/Si alloy, whilst for Mn-first alloys it remained unchanged (6%) by the dimensions 404 and 430 μm, and by standard deviations σ=17.9 μm and 20.3 μm. In both alloys, where pre-eutectic phases occurred (Table 2), number density n_{Mn} decreased, 10% and 65%. Analyzing cross-section of the sample (Figure 2), for Mn-first (AlSi12.546Mn1.011) alloy, $Al_{15}Si_2Mn_4$ phases are larger (510 μm) inside (area A) then outside (area D, 368 μm), both without and with electromagnetic stirring. For both, natural and forced convection, number density n_{Mn} was higher inside sample (area A) than outside (area D). Opposite situation was noticed for Mn/Si alloy, where more and larger phases occurred in outer part of sample, where flow increased dimension L_{Mn} and decreased number density n_{Mn}. In Tables 2-4 used dash "-" indicates a lack of intermetallics, crystals or dendrites in the area and resulting number density value of 0.0 mm^{-2}.

The average length L_{Si} of Si-crystals (Table 3) decreased under stirring by 17% in the Si-first and increased 15% in the Si-2-first alloy, while the number density n_{Si} decreased considerably by 52% and 75% in both alloys. Analyzing cross-section of the sample, larger Si crystals were noticed in the outer part than inside, as also seen on Figures 5,7 and 8. For the Mn/Si alloy, L_{Si} increased slightly by 9% from 1202 to 1306 μm, while n_{Si} decreased by 81%.

For the Mn-first and Si-first alloys (Table 4) the stirring caused 13% and 38% increase in secondary dendrite arm spacing λ_2, from 75.2 μm to 85 μm and from 29 μm to 40 μm respectively. In areas from A to D, across the specimen, when considering the standard deviation, λ_2 seems to have similar various values. Specific surface S_V decreased for mentioned alloys 29% and 22% respectively.

Table 1.
Parameters characterizing inter-eutectic Mn phases and Al-Si eutectics

Aluminum Alloys	RMF [mT] {Solid. Time [s]}	Mn phases (inter-eutectic – small phases)		AlSi Eutectics
		L_{Mn} [μm]	n_{Mn} [mm^{-2}]	λ_E [μm]
"Mn-first" alloy AlSi12.546 Mn1.011	0{468}	47.88 [4.770] (219) 17.57:87.06:24.55:40.61 [1.16:5.43:1.75:3.04]	83.42 80.75:126.5:99.04:27.42	9.09 [0.87] 8.4:5.4:10.2:13.9
	11{504}	26.94 [1.829] (248) (-44%) 31.51:18.54:30.64:35.49 [2.01:1.15:2.19:1.50]	94.46 (13%) 112.7:143.2:73.13:48.75	8.88 [1.70] (-2%) 6.0:5.1:8.9:20.6
"Si-first" alloy AlSi14.732 Mn0.567	0{606}	29.67 [2.221] (270) 18.16:35.77:39.71:48.65 [1.08:1.97:2.72:3.13]	102.8 188.9:129.5:42.69:50.28	12.65 [2.51] 6.2:8.5:21.0:27.1
	11{646}	28.62 [2.005] (188) (-4%) 19.96:32.75:32.37:34.24 [0.92:2.42:2.25:1.55]	71.61 (-30%) 94.46:108.1:53.32:30.47	15.32 [2.10] (21%) 9.2:10.3:24.4:24.5
"Si-2-first" alloy AlSi16.050 Mn0.558	0{566}	16.07 [1.257] (281) 9.68:14.19:23.19:33.08 [0.62:0.82:1.23:1.92]	107.0 173.3:124.9:86.84:42.66	11.43 [2.45] 3.7:8.9:18.8:25.6
	11{391}	9.98 [0.610] (351) (-38%) 8.24:7.96:12.08:13.45 [0.39:0.35:0.76:0.76]	133.7 (25%) 141.7:164.5:158.5:70.08	5.52 [0.66] (-52%) 3.0:4.8:7.0:8.6
"Mn/Si" alloy AlSi14.870 Mn1.159	0{516}	38.03 [5.65] (275) 25.69:43.77:70.70:88.51 [2.32:5.02:11.01:10.99]	104.7 269.7:77.72:41.13:30.47	12.70 [1.63] 7.0:9.0:13.8:22.9
	11{558}	20.22 [2.52] (491) (-47%) 25.06:26.38:36.60:46.92 [1.89:2.18:4.01:3.50]	187 (79%) 248.3:184.3:65.5:35.0	13.93 [2.34] (10%) 7.4:10.2:13.4:27.3

(1) Dash – lack of data e.g. by absence of phases; (2) Brackets [the standard deviation]; (3) Parentheses (numbers of grains inspected/numbers of dendrite arms counted) ; (4) Curly brackets {the solidification time (s)}; (5) Parentheses (caused by forced flow variation [%] of the parameters %); (6) Parameters separated by colon : – values gained in areas A,B,C and D.

3.3. Precipitation sequence

The alloys compositions precisely meeting the methodology assumptions, were defined using thermodynamic calculation [25]. The determined precipitation sequence and mass fraction of the occurring phases were collected in Table 5 and for example of Mn-first alloy discussed below and showed on Figure 9.

For the alloy where $Al_{15}Si_2Mn_4$ should be the first growing phase, based on the ternary Al-Si-Mn phase diagram (Figure 1), the composition AlSi12Mn1 was proposed. Next according to iterative calculations, with property diagram (Figure 9) and Scheil solidification, carried out analysis gave the alloy with exact AlSi12.546Mn1.011 composition. In the alloy (Table 5), starting from liquidus temperature 610 °C and according to reaction described as L → $Al_{15}Si_2Mn_4$ + L, $Al_{15}Si_2Mn_4$ phase will form. Similarly to growth of solid Mn phases and during it, the melt enriches in Mn and Si, and the concentration amounts 0.591%Mn and 12.569%Si finally at the temperature 575.89 °C. At this temperature and Mn and Si concentrations, the solidification path reached eutectic grove and followed the reaction L → L + $Al_{15}Si_2Mn_4$ + Si till 575.88 °C, where finished with composition of rest liquid 12.570%Si and 0.582%Mn. At this point and temperature 575.88 °C, occurred L → α-Al + $Al_{15}Si_2Mn_4$ + Si as the final eutectic reaction, where mass fraction of $Al_{15}Si_2Mn_4$ reaches $f_{Al15Si2Mn4}$ = 3.12%, α-Al mass fraction $f_{\alpha\text{-}Al}$ = 85.99% and eutectics mass fraction reaches f_{Eut} = 10.89%. From precise iterative calculations resulted non-intentionally L → L + $Al_{15}Si_2Mn_4$ + Si reaction, that occurred during very short temperature range, from 575.89 °C to 575.88 °C, and has got only numerical meaning, but from practical view of alloys preparation

has no importance. The planed two reactions L → $Al_{15}Si_2Mn_4$ + L and L → α-Al + $Al_{15}Si_2Mn_4$ + Si occurring during much longer temperature range 610-575.89 °C than 575.89-575.88 °C practically fulfilled the main idea of current study.

4. Discussion

Based on the solidified samples received from natural only convection and from forced convection, the discussion on the microstructure modification is possible. The changes in distribution and dimensions of intermetallics, Si crystals, eutectics and α-Al phase, captured by figures and measured parameters will be analyzed.

4.1. Mn-phases

$Al_{15}Si_2Mn_4$ Mn-rich phases occurs also in more complicated alloys than analyzed in the current study, e.g. in AlMgSi [20] and AlCuSi [21] alloys, and also the stirring effect on morphology was also earlier studied for directional solidification of AlSiMn alloys [2]. The analysis by low gradient or directional solidification of AlSiFe alloys may show some microstructure modifications.

Table 2.
Parameters characterizing pre-eutectic Mn intermetallics

Aluminum Alloys	RMF [mT] {Solid. Time [s]}	Mn phases (PRE-eutectic – large phases)	
		L_{Mn} [μm]	n_{Mn} [mm^{-2}]
"Mn-first" alloy AlSi12.546Mn1.011	0{468}	404 [17.9] (211) 510:464:389:368 [33.8:17.9:14.3:16.9]	0.372 0.367:0.386:0.496:0.278
	11{504}	430 [20.3] (189) (6%) 592:340:432:443 [21.6:16.7:19.5:20.2]	0.333 (-10%) 0.508:0.395:0.384:0.246
"Mn/Si" alloy AlSi14.870Mn1.159	0{516}	382 [17.5] (211) -:227:376:396 [-:9.2:19.8:16.3]	0.372 0.0:0.084:0.355:0.561
	11{558}	616 [65.4] (68) (61%) -:-:304:652 [-:-:7.3:68.1]	0.120 (-68%) 0.0:0.0:0.0395:0.246

Table 3.
Parameters characterizing Si crystals

Aluminum Alloys	RMF [mT] {Solid. Time [s]}	Si crystals	
		L_{Si} [μm]	n_{Si} [mm^{-2}]
"Si-first" alloy AlSi14.732Mn0.567	0{606}	1342 [101.9] (123) -:755:1362:1361 [-:46:86:108]	0.217 0.0:0.038:0.169:0.359
	11{646}	1119 [76] (59) (-17%) -:-:-:1119 [-:-:-:76]	0.104 (-52%) 0.0:0.0:0.0:0.238
"Si-2-first" alloy AlSi16.050Mn0.558	0{566}	1482 [129] (82) -:-:1044:1721 [-:-:45:152]	0.145 0.0:0.0:0.163:0.214
	11{391}	1704 [90] (20) (15%) -:-:-:1704 [-:-:-:90]	0.036 (-75%) 0.0:0.0:0.0:0.081
"Mn/Si" alloy AlSi14.870Mn1.159	0{516}	1202 [121] (156) -:-:1376:1174[-:-:91:125]	0.275 0.0:0.0:0.118:0.544
	11{558}	1306 [114] (30) (9%) -:-:-:1306 [-:-:-:114]	0.053 (-81%) 0.0:0.0:0.0:0.121

The average overall dimension L_{Mn} of Mn-phases decreased 9% under melt flow in AlMg5Si5Mn1 alloy [20] where $Al_{15}Si_2Mn_4$ precipitate (solidify) as first before eutectics and α-Al, by low gradient and slow cooling. And similarly in the AlCu4Si6Mn2 alloy [21] where $Al_{15}Si_2Mn_4$ grow as first, L_{Mn} decreased 19%. Whilst for Mn-phases starting to precipitate 17 ˚C after α-Al, and as the second, by lower Mn contain (AlCu4Si6Mn0.65 alloy) [21], and by common growth till final eutectic reaction, convection reduced the length L_{Mn} by 42%. For AlSiMn alloys [3], the inter-eutectic phases (being part of ternary eutectics) were larger under stirring, whilst pre-eutectic intermetallics grew smaller. For lower Si and Mn content [3], the changes were unclear for inter-eutectic phases, whilst pre-eutectic phases solidified smaller.

For Fe-rich intermetallics, the complete destruction in case of AlSi7Mg0.2–0.6Fe0.5 alloy or significant 80% decrease in the dimension of β-Al_5FeSi, caused by stirring was observed [32]. The modification of phases depends on cooling conditions, in metal mold the reduction was small, but in sand mold the length $L_β$ of β needles reduced about 23% [27]. Flow leading to segregation may also cause increase in length of β from 160 μm 280 [28], in AlSi7Fe1.0 alloy solidified directionally. In similar to [28] experiment [29], formation of eutectic rich center was presented with 9% larger needle shaped Fe phases, but also 20% reduction in dendritic structure was observed. The flow effect

depends also on the presence of other phases, e.g. Mg_2Si in AlMgSiFeMn alloys [20] may reduce stirring influence on dendrites, intermetallics and eutectic. The importance of alloy composition was presented in case of AlCuSi system [21], where for AlCu4Si6Fe1 alloy 33% reduction in length was noticed, whilst the increase 76% and 23% for AlCu4Si6Fe2 and AlCu10Si10Fe1 alloys where β-Al_5FeSi needles grow as first precipitate. As demonstrated in [29] on histograms, flow led to higher amount of small phases (5-40 μm) and finally caused smaller average length of the whole population of intermetallics. The importance of precipitation sequence for flow efficiency in reduction of iron phases [29], was noticed in [19], where in the presence of α-Al phases flow reduced 14% the length in AlSi7.837Fe0.521 alloy, whilst in fully liquid alloy, with only precipitating β-Al_5FeSi, the length increased 92% and 76%, in slowly cooled by low temperature gradient, AlSi12.795Fe1.705 and AlSi12.911Fe2.372 alloys. The results [29] suggested the influence of similarly growing α-Al on L_β reduction, whilst in AlSi7.508Fe1.687 alloy [19] the 17% increase was noticed. By joint growth of Si crystals and β-Al_5FeSi, in the AlSi15.136Fe1.678 alloy [19], the 22% decrease in L_β was observed, that confirms the reduction effect of the second occurring phase. In both alloys, the mass fraction of solid phases precipitated differs, there is less solid Si crystals in AlSi15.136Fe1.678 than α-Al in AlSi7.508Fe1.687 alloy. The mass fraction of solid phases influences flow possibility in mushy.

Table 4.
Parameters characterising α-Al phases

Aluminum Alloys	RMF [mT] {Solid. Time [s]}	α-Al phase (dendrites or globular forms)	
		λ_2 [μm]	S_v [μm^{-1}]
"Mn-first" alloy AlSi12.546Mn1.011	0{468}	75.2 [16.0] (13/91) 157:112:70:60 [-:7.7:5.8:6.7]	0.034 [0.008] 0.038:0.033:0.032:0.035 [0.005:0.002:0.003:0.013]
	11{504}	85 [12] (14/84) (13%) 124:70:86:83 [4.6:8.6:13.4:9.0]	0.024 [0.002] (-29%) 0.030:0.024:0.025:0.022 [0.002:0.002:0.001:0.001]
"Si-first" alloy AlSi14.732Mn0.567	0{606}	29 [1.4] (10/91) 21:31:42:71 [1.4:2.0:-:-]	0.040 [0.005] 0.075:0.041:0.039:0.026 [0.005:0.005:0.001:0.002]
	11{646}	40 [4.7] (5/26) (38%) 25:44:38:46 [-:1.1:-:-]	0.031 [0.006] (-22%) 0.052:0.040:0.027:0.028 [0.004:0.002:0.002:0.007]
"Si-2-first" alloy AlSi16.050Mn0.558	0{566}	35 [6.1] (6/39) 31:30:87:42 [6.1:-:-:-]	0.036 [0.003] 0.083:0.044:0.039:0.029 [0.003:0.013:0.004:0.006]
	11{391}	22 [3.6] (8/112) (-37%) 24:26:31:19 [5.0:-:4.4:3.8]	0.066 [0.008] (83%) 0.090:0.089:0.054:0.059 [0.008:0.016:0.003:0.005]
"Mn/Si" alloy AlSi14.870Mn1.159	0{516}	32 [7.3] (6/40) 19:45:50:75 [1.4:3.0:-:-]	0.031 [0.006] 0.060:0.050:0.031:0.024 [0.006:0.007:0.008:0.001]
	11{558}	35 [3.6] (6/32) (9%) 20:42:40:58 [3.6:0.2:-:-]	0.031 [0.007] (0.0%) 0.044:0.053:0.031:0.025 [0.007:0.007:0.003:0.003]

Table 5.
Precipitation sequence in studied AlSiMn alloys

Alloy	Reaction	Temperature Range of Reaction	Mass Fraction of Solid Phases [%] (the Rest is Liquid Alloy) at the Temperature [°C]				
			Temperature	α-Al	$Al_{15}Si_2Mn_4$	Si crystals	Al-Si Eutectics
"Mn first" alloy AlSi12.546Mn1.011	L → $Al_{15}Si_2Mn_4$ + L	610–575.89	575.89	0	1.47	0	0.0
	L → α-Al + $Al_{15}Si_2Mn_4$ + Si	575.89–575.88	575.88	85.99	3.12	0	10.89
"Si first" alloy AlSi14.732Mn0.567	L → Si + L	610–575.89	575.89	0.0	0.0	2.39	0
	L → α-Al + $Al_{15}Si_2Mn_4$ + Si	575.89–575.88	575.88	85.12	1.64	2.47	10.77
"Si-2 first" alloy AlSi16.050Mn0.558	L → Si + L	630–575.89	575.89	0	0	3.91	0
	L → α-Al + $Al_{15}Si_2Mn_4$ + Si	575.89–575.88	575.88	83.80	1.61	3.98	10.61
"Mn/Si" alloy AlSi14.870Mn1.159	L → $Al_{15}Si_2Mn_4$ + Si + L	610–575.89	575.89	0.0	2.03	2.67	0
	L → α-Al + $Al_{15}Si_2Mn_4$ + Si	575.89–575.88	575.88	83.18	3.63	2.70	10.49

The amount of formed intermetallics modified under flow was characterized by counting number density n_{Mn}. Forced flow caused 30% increase in number density n_{Mn} in AlMg5Si5Mn1 alloy [20], where Mn phases grow as first, and 53% in

AlCu4Si6Mn0.65 alloy [21], but here Mn-rich precipitates start to grow 17 ˚C after α-Al. For AlCu4Si6Mn2 alloy [21], stirring caused 41% decrease in n_{Mn} where $Al_{15}Si_2Mn_4$ grow as first.

For processed in sand mold AlSi6.8Fe0.8 alloy [27] amount of iron-rich phases increased about 100%, whilst in metal mold only slightly. Both in the dendritic outside area (17%) and in the eutectic center (42%) of directionally solidified cylindrical samples, number density n_β increased. The presence of Mg_2Si [20] in AlMgSiMn alloys seems to reduce flow and its effect on number density modification. The number density n_β decreased under flow, 12 and 71 %, in AlCu10Si10Fe1 and AlCu4Si6Fe2 [21] respectively, where β-Al_5FeSi start to grow as first, and n_{Mn} increased in AlCu4Si6Fe1 where Fe-phases precipitated (solidified) as the second and α-Al as first. In AlSi12.795Fe1.705 and in AlSi12.911Fe2.372 alloys [19], where β needles grow as only one from liquidus till eutectic temperature, n_β decreased 71% and 70% respectively, whilst n_β increased 130% in AlSi7.837Fe0.521 alloy where β-Al_5FeSi precipitate between dendritic or globular formed α-Al phase, and confirmed results found out in directional solidification [29]. By joint growth of β-Al_5FeSi and Si crystals [19], n_β decreased 45% and by joint growth of β-Al_5FeSi and α-Al n_β decreased 26%, and that is in contrary with [29].

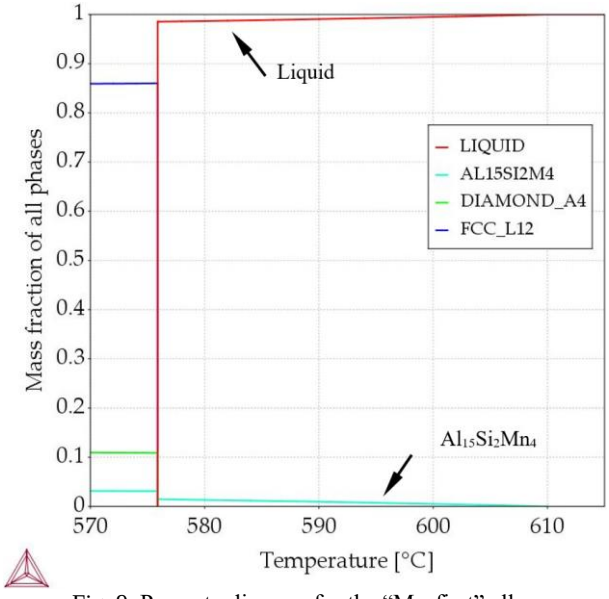

Fig. 9. Property diagram for the "Mn-first" alloy (AlSi12.546Mn1.011)

The measurement of Mn-phases in current study was divided into pre-eutectic (Table 2) and inter-eutectic (Table 1) phases. Pre-eutectic manganese phases have dimensions in the range about L_{Mn} = 382-616 μm by number density n_{Mn} = 0.120-0.372 mm^{-2}, while inter-eutectic L_{Mn} = 9.98-47.88 μm by number density n_{Mn} = 71-133 mm^{-2}.

The inter-eutectic Mn phases (Table 1), being part of ternary eutectics, precipitate (solidify) in the final eutectic reaction, together with α-Al, Si crystals, and Al-Si eutectics, and may lead to dumping the flow at this solidification stage. For Mn-first alloy, convection caused 44% (Table 1) smaller Mn-phases by 13% slightly increased umber density. In Si-first and Si-2-first alloys, stirring caused smaller inter-eutectic Mn-phases, the average dimension L_{Mn} decreased 4% and 38% respectively. For Mn/Si alloy, Mn phases changed under flow similarly to Mn-first alloy, L_{Mn} decreased 47%. In case of the precipitation between earlier formed phases and late growth, similar reaction of inter-eutectic Mn phases to flow seems clear.

The pre-eutectic Mn phases precipitate (solidify) by joint growth with Si crystals (Si/Mn alloy, Table 2) or separate (Mn-first alloy). In the Mn-first alloy (Table 2), flow caused 6% larger pre-eutectic phases by 10% decreased number density. The common growth of Mn and Si crystals (Mn/Si alloy) led by forced flow to 61% larger Mn phases and its 68% lower number density. For the growth of Mn phase in alloys with at the beginning only small amount of solid phases, Mn-first and Mn/Si alloys, where both grow in almost completely liquid alloy, opposite effect concerning dimension L_{Mn} was found. Because of the fulfilled with liquid alloys solidifying specimen, by absence of dendrites of globular forms and its large value of mass fraction, Mn grew freely in liquid alloy, and similar effect should be observed. It seems that some effect may come from Si crystals presence or from Si and Mn concentration in alloys. Probably Si is the key element for flow effect in these alloys, in meaning hypo or hypereutectic alloys. Number density across specimen has also importance and shows different effects. The lack of α-Al (Mn-first and Mn/Si alloys), flow caused decrease in number density stronger in the specimen center (area A and B), e.g. decreasing from 0.084 to 0.0395 (Mn/Si alloy) and slighter and more uniform in Mn-first alloy. The mentioned decrease in number density of Mn phases for these alloys is significant. For Mn-first alloy, across sample diameter, number density has higher values in the center than outside, for Mn/Si alloy the opposite situation was found, both without and with stirring. Such situation seems clear according to phases diagram and real solidification front movement from crucible into center, even in such slow cooling and small gradient, where the distribution of phases in eutectic (Mn-first) alloy is opposite to hypereutectic (Mn/Si) alloy. Forced flow seems to keep this course of number density across sample, by generally lower values with flow, but for Mn-first alloy, forced convection caused increase from 0.367 to 0.508 mm^{-2} in number of phases in the center. For Mn/Si alloy with applied stirring, the center, areas A and B, are empty of Mn-phases, n_{Mn} = 0.0 mm^{-2}.

The 6% increase in the overall dimension L_{Mn} is the opposite of 9% decrease for AlMg5Si5Mn1.0 alloy [20] by similar temperature gradient and cooling rate, where $Al_{15}Si_2Mn_4$ precipitate at T_L = 651 ˚C till 606 ˚C as first. L_{Mn} stayed unchanged in AlCu4Si6Fe1Mn0.65 alloy [21], where start to grow by T_L = 625 ˚C, and number density reduced 56% similarly to Mn-first alloy. For Mn/Si alloys, no results measuring flow effect on Mn phases by joint growth was found. Instead, for joint growth of α-Al starting at T_L = 610 ˚C and Mn phases at 593 ˚C in AlCu4Si6Mn0.65 alloy [21], the opposite situation was found, number density increased 53% and the average dimension L_{Mn} decreased 42%. Both alloys clearly differs in the mass fraction of α-Al in comparison to Si crystals.

4.2. Si crystals

In the Si-first, Si-2-first and Mn/Si alloys (Figure 5,7 and 8), two different areas are clearly visible, the internal areas A and B without Si crystals and the external areas C and D which is rich with Si crystals (Figure 2). This observation was confirmed by measurement of overall dimension and number density of Si crystals, e.g. for Si-first alloy, in center (area A) number density amounts 0.0 mm^{-2}, while in outside (area D) 0.359 mm^{-2} without flow and 0.0 and 0.238 mm^{-2} with flow, respectively. In mentioned alloys, stirring moved Si crystals from areas C and D, including space from 50% of sample radius (0.5 R) to the edge, to the outside area D including space from 75% of radius (0.75 R) to the edge (Figure 5,7 and 8). Forced flow decreased significantly amount of occurring crystals, number density was lower 52%, 75% and 81 % respectively for Si-first, Si-2-first and Mn/Si alloys (Table 3). The sample center is filled mainly with α-Al-Si eutectics. In all mentioned alloys, without and with stirring, larger Si crystals grew near to sample edge, and smaller nearer to center, e.g. for Si-2-first alloy, without stirring L_{Si} in area C was 1044 μm and in area D 1721 μm, while convection moved them all outside (to area D) by L_{Si} 1704 μm. For Si-first alloy, without stirring L_{Si} in area C was 1362 μm and in area D 1361 μm, while convection moved them all outside (to area D) by L_{Si} 1119 μm. In the Mn/Si alloy, under stirring, the Si crystals grew 9% larger with a 81% reduction in the number density. The largest Si crystals precipitated (solidified) in the thin outside layer (area D), and crystals also moved to the center (area A) and to the edge of the sample (area C), with the highest number density of 0.121 mm^{-2}.

Forced flow generated by coils definitely influenced the growth site of Si crystals and significantly reduced number density in samples where Si crystals precipitate first and also in the Mn/Si alloy, where joint growth occurs. It seems that flow pushed Si crystals to grow less as separate Si crystals and more as α-Al-Si eutectics, which may positively influence alloy properties and castings quality.

The separation of Si crystals in an Al-30 wt.% Si alloy under RMF was studied in [30], where by stirring the Si crystals were located in a thin layer of about 8 mm and also in the sample center in contrast to current study (Figure 5,7,8). In opposite to current observations, along the cylindrical sample also Si segregation may occur as studied in an Al-Si 45 wt.% Si alloy [31] by temperature gradient 35-40 K/cm or as in directional solidification of Sn-Si alloy [32] or in a Ti-85 wt.% Si alloy [33]. In the current study only electromagnetic stirring by RMF was applied, but also mechanical stirring [34] may lead to Si separation and even alloy purification from phosphorus and boron [34, 35] by increased average mass and size of primary Si flakes [35].

The applied in current study electromagnetic stirring generate fluid flow, but also direct application of electric current, as e.g. electric current pulse ECP may cause changes in Si concentration [36], eutectic spacing [37] and the removal of boron but by directional solidification. In opposite to low gradient and low cooling rate applied in the current study, application of high temperature gradient or pulling the sample, may lead to Si segregation in upper [38] or lower [39] part of samples together with removal of P, B, Ca, Fe [40]. The current methodology assumed constant electromagnetic field 11 mT, but alternating electromagnetic directional solidification (AEM-DS) [41] in an Al-45 wt.% Si alloy caused Si separation in the bottom part of sample and upper part rich in eutectics and only small layer of Si on the sidewall. The construction of the facility used in this study, allowed for only still, not moving sample in graphite crucible, but Jiang et al. [42] and Xue et al. [43] observed that pulling down resulted in Si crystals in the bottom of sample and pulling up led to upper part significantly enriched in Si crystals in various AlSi alloys. In the current study constant electromagnetic field in strength of 11 mT was applied, but application of the gradient high magnetic field by Li, Ren and Fautrelle [44] separated primary Si and the Si solute, moved α-Al and the eutectics towards the down part of the sample, whilst the primary Si phase moved towards the top. The applied by Sun et al. [45] in an Al-30 wt.% Si-10 wt.% Sn alloy a traveling magnetic field (TMF) caused that a binary eutectic α-Al+Si formed in the upper and in the center parts of the sample.

In a three-phase-three-pole magnetic generator (RMF 25 mT) applied for solidification of a 60 mm diameter cylindrical sample, Zou et al. [46] tried to control behavior of primary Si and the segregation in an Al-30 wt.% Si alloy, and observed that for the realization of Si separation, the temperature gradient is a precondition. Secondly, electromagnetic stirring forming a Si-rich layer with 65~70 wt.% Si content, can strengthen the separation effect for Si but is not decisive. In the current study the cooling rate achieved 0.574 K/s and the temperature gradient was 0.238 K/mm whilst in [46] the temperature gradients were 1.5/0.3 ˚C/mm and 0.5 ˚C/mm and the cooling rates were 1.5 ˚C/min (0.025 ˚C/s) and 60 ˚C/min (1 ˚C/s) and seems to confirm the current study. In current solidification without RMF, a lower gradient was measured (0.238 K/mm) and the separation of Si occurred in the outer part of the sample (Figure 5,7 and 8) and RMF decreased the number density of Si particles. The cooling rate measured currently matches the range presented in [46]. Based on the numerical simulation, Zou et al. [46,47] suggested that RMF caused the formation of a primary azimuthal flow and then in the azimuthal direction a secondary flow, finally transporting of solute atoms in the axial direction. The authors [48] also proposed a method for the Si purification.

4.3. Eutectics

The mechanism of eutectics formation [49,50] includes the growth of two or three phases by diffusion and without any exchange of solute between solids. From solidified phases rejected solute moves into liquid located near to solid phases and the concentration and location of solute may depend on melt flow. The eutectic spacing first depends on materials and on the solidification velocity [50,51]. Secondly, the spacing may depend on the flow, as was observed in unidirectionally solidified AlSi alloys [52], where the spacing increased from 4 μm by natural only convection to 8 μm when an electromagnetic field of 6 mT was present. The flow near final solidification may be reduced by e.g. Mg_2Si phases as found out in AlMgSiFeMn alloys [20] studied by similar to current methodology. And as confirmed in similar equiaxed solidification of AlCuSiFeMn alloys [21] by low cooling rate and low temperature gradient, the eutectic spacing correlation to forced convection depends on the alloy composition.

In Mn-first alloy [Table 1], the changes in eutectic spacing λ_E are -2% and by standard deviation of σ=0.87 and 1.70 μm, the changes appear negligible. In the Mn-first alloy, the amount of eutectics in comparison to e.g. hypoeutectic alloys with profusely occurring α-Al is large, and eutectics form without dense globular or dendritic structures where the flow might be diminished.

For the Si-first and Si-2-first alloys [Table 1] the changes 21% and -52% show probably different effect of the flow. Also in this hypereutectic alloys, the amount of solid phases precipitating before eutectics is small. The mass fraction of Si crystals [Table 5], at final eutectic reaction amounts 2.47% and 3.98% respectively, and both values are small in comparison to some hypoeutectic alloys where mass fraction of α-Al amounts 85-96%. The overall dimension of Si crystals in both alloys is similar, in the range 1119-1342 μm for Si-first and 1482-1704 μm for Si-2-first alloys. The flow conditions seems to be at least similar if not identical in both alloys.

For the Mn/Si alloy λ_E increased 10%, and by standard deviation of σ=1.63 and 2.34 μm, the changes are negligible. The amount of eutectics is large in comparison to the Si crystals and Mn phases (Table 4), the mass fraction of Si crystals [Table 5] amounts 2.70 and Mn-phases 3.63. The overall dimension of Si crystals is in the range 1202-1306 μm [Table 3] and of pre-eutectic Mn-phases 382-616 μm [Table 2].

The morphology of solid-liquid mushy zone in studied alloys seem to be very convergent but measured eutectic spacing [Table 1] do not imitate this situation. The electromagnetic field is still present in the material till final solidification and can generate flow in any small liquid cavities that may still be present between already solidified grains. The unclear effect of forced convection on studied AlSiMn alloys during slow cooling and low temperature gradient demand more further investigation, including smaller specimen sizes and stronger stirring by mechanical or electromagnetic methods.

4.4. α-Al crystals

In the studied alloys, intentionally and according to phases diagram, not any dendrites or globules should form. But some composition fluctuation caused α-Al crystals formed as globular forms or fully shaped dendrites.

The intensive forced flow may lead to microstructure with spheroidal forms precipitating in mushy zone, as presented by Flemings [53]. Many other experimental studies on e.g. metallic AlCu alloys [54-56], water succinonitrile (SCN)-5% [57] or in modelling and numerical simulations [58], have investigated the phenomena of structure transformation by flow.

For equiaxed grain morphologies formed by equiaxed solidification without flow, the microstructure is characterized among others by secondary dendrite arm spacing $\lambda_2 = \lambda_{SDAS}$. Assumption, that dendrite growth is diffusion-controlled, has led to mathematical model [51]:

$$\lambda_2 = c_1 \cdot t^{n1} \tag{1}$$

where n_1 = 0.48 for convective and 0.33 for the diffusive mass transport [52] and c_1 materials depending coefficient [51].

For the Mn-first alloy (Table 1), the stirring increased 13% secondary dendrite arm spacing λ_2, from 75.2 μm to 85 μm and by standard deviation of σ=16 and 12 μm, the changes appear small. For the Si-first and Si-2-first alloys (Table 1) the flow caused an approximate 38% and -37% changes in λ_2, from 29 μm to 40 μm and from 35μm to 22 μm respectively. For Mn/Si alloy, λ_2 increased 9% from 32 μm to 35 μm and by σ=7.3 and 3.6 μm, the changes appear small.

Throughout the Si-first and Si-2-first specimens (Table 1), in areas from A to D (Figure 2), λ_2 seem to have various values when considering the standard deviation σ, but no clear tendency was observed. For Mn-first alloy larger spacing λ_2 occurred in the center of the cylindrical sample, whilst in the Mn/Si opposite tendency was observed.

For the Mn-first and Si-first alloys, according to equation (1), the solidification time and the measured secondary spacing λ_2, in order to achieve calculated λ_2 values equal to the measured ones, the exponent n_1 by stirring should be higher, increasing from 0.33 for diffusive mass transport, to values such as 0.3455 and 0.376 respectively, for convective ripening, and this is much smaller than the values of 0.47–0.50 found in the literature [52] for directional solidification. For the Si-2-first alloy, the contrary situation was found, flow caused smaller λ_2 and that means n_1 by stirring should be lower, 0.275, even lower than for diffusive ripening 0.33. For the Mn/Si alloy n_1 changed from 0.33 to 0.3405. The value increased but is smaller than the values of 0.47–0.50 found in the literature [52].

The value of exponents suggests a small or even a lack of forced flow by electromagnetic field or the flow reduction during the secondary arms coarsening. The mass fraction of Si crystals and Mn phases is smaller than that of α-Al, as seen in the Figures 3,5,7 and 8, property diagram (Figures 9) and Table 5. In opposite to any hypoeutectic alloys with overwhelming α-Al phase, in the currently studied alloys appear to be better conditions for long lasting and intensive melt flow.

Another parameter proposed [59] for grain characterization is the specific interfacial area S_v proportional to the solidification time t:

$$S_V \sim t^{-1/3} \tag{2}$$

and its value S_v may decrease from 0.077 to 0.035 μm^{-1} with increasing electromagnetic stirring in AlCu30 alloy [60].

The specific surface S_v decreased (Table 1) under stirring for the Mn-first and Si-first alloys by 29% and 22% respectively, much more than the standard deviation range. Only for the Si-2-first S_v increased by 83%, which is consistent with changes in λ_2. For the Mn/Si alloy flow has not changed Sv. The values throughout the specimen, in areas A-D (Figure 2), are almost equal for Mn-first alloy, whilst for Si-first, Si-2-first and Mn/Si alloys decreased from area A to D.

Based on the measured solidification time, calculation of S_v according to (2) need determination of a coefficient describing the proportionality. The coefficient for currently studied AlSiMn alloys amounts 0.2317-0.4281 for solidification by only natural convection and 0.1427-0.4813 for stirring. S_v changes more significantly than λ_2 and seems to signal flow better.

4.5. Solidification by stirring

For the Mn-first (AlSi12.546Mn1.011) alloy, in comparison to natural convection, stirring decreased L_{Mn} of inter-eutectic Mn-phases 44% and increased n_{Mn} by 13%. For pre-eutectic Mn-phases flow increased L_{Mn} by 6% and decreased n_{Mn} by 10%. By the standard deviation of σ=17.9 µm and 20.3 µm the changes are small. Based on the calculations in Thermo-Calc (Figure 1), the first and only one is pre-eutectic Mn-phase, growing from liquidus till solidus temperature. In the fully liquid alloy, the manganese-rich growing phase seems to have the perfect conditions to reach large dimensions, and the reaction much weaker than in case of β-Al_5FeSi [19], where increase amounts 92% and 76% depending on alloy composition. It seems, flow has no influence on the dimension and position across sample, because by natural only and forced convection, longer Mn-phases formed in the center (area A) by higher number density, than in the outside (area D). For AlMg5Si5Mn1.0 alloy [20], where Mn-rich phase starts to precipitate first with T_L = 651 ˚C till 606 ˚C, decrease in L_{Mn} was observed, and perhaps the liquidus temperature is too low in Mn-first alloys, for such an effect.

In the samples of Si-first and Si-2-first alloys flow changed the secondary spacing λ_2, specific surface S_v and the eutectic spacing. For the Si-first and melt stirring decreased the average length L_{Si} of Si crystals by 17% and decreased the number density n_β by 52%, whilst for Si-2-first alloy, L_{Si} increased 15%, and n_β decreased by 75%. According to thermodynamic calculations (Figure 1), the Si crystal is the first and only growing phase until the eutectic reaction. In the fully liquid alloy, the Si crystal growing first appears to have the great conditions to reach large size, by the absence of dendritic or globular α-Al. In similar alloys [21] (Al–Si14.877Fe0.871 and Al–Si16.187Fe0.858), L_{Si} increased by 17% and 20%, and n_β decreased by 89% and 74%, respectively. Electromagnetic stirring leads to a significant reduction in the number of Si crystals present and a definite reduction in their growth area, pushing Si to the edges of the samples (Figure 5,7 and 8).

For the Mn/Si alloy, stirring induced by coils, increased λ_2 by 9%, surprisingly S_v did not changed, increased λ_E by 10%, increased L_{Mn} of pre-eutectic Mn-phases by 61% and decreased n_{Mn} by 68%, increased L_{Si} by 9% and significantly decreased n_{Si} by 81%. Based on the calculations in Thermo-Calc (Figure 1), Mn-phases and Si crystals grow together along the monovariant line (continuous blue line on Figure 1) from liquidus temperature of 610 ˚C till solidus at 575 ˚C. Because the final mass fraction of Mn-phases and Si-crystals reaches 3.63% and 2.70% and of Al-Si eutectics 10.49%, the phases grow freely in almost fully liquid till final eutectic reaction. This allows for large Mn-phases and Si crystals, by its significantly smaller amount and the movement into the outside of cylindrical sample.

In AlMg5Si5Mn1.0 alloy [20] with liquidus temperature T_L = 651˚C and Mn-phases precipitating as first, the overall dimension of Mn-phases decreased 9% and number density increased 27%, whilst in current Mn-first alloys L_{Mn} increased 6% and number density decreased 10%. Generally, the changes are small, but when omitting standard deviations value, some opposite reactions to flow might be observed. In AlCu4Si6Fe1Mn0.65 alloy [21] L_{Mn} did not changed and n_{Mn} decreased 56% by T_L = 625 ˚C and Mn-phases precipitated (solidified) first. In AlCu4Si6Mn0.65 alloy [21], L_{Mn} decreased 42% and n_{Mn} increased 53% by T_L = 610 ˚C and Mn-phases precipitated after α-Al. It seems that Mn phase became smaller (e.g. 42%) when precipitated as the second after α-Al crystals, and stayed almost unchanged when precipitate first and this is similar to β-Al_5FeSi phases [19-21,29,61] in AlSiFe alloys. Mn-phases in eutectic Mn-first alloy do not segregate and do not change location across sample and results agree with flow effect on β-Al_5FeSi phases [19]. Whilst in hypereutectic Mn/Si alloy, by joint growth with Si crystals, L_{Mn} increased, n_{Mn} decreased significantly, and also Mn-phases moved slightly to outside of sample.

It seems that overall dimension L_{Mn}, decreased in hypoeutectic alloys, by presence of α-Al (e.g. AlCu4Si6Mn0.65 alloy [21]), stays almost unchanged in eutectic alloys (e.g. Mn-first alloy) or when Mn-phases precipitate first (AlCu4Si6Fe1Mn0.65 alloy [21]), and L_{Mn} increases in hypereutectic alloys by joint growth in presence of Si crystals (e.g. Mn/Si alloy).

In similar to current study experiments, the separation of Si crystals in an Al-30 wt.% Si alloy under RMF was studied [30], where by stirring the Si crystals were located in a thin layer of about 8 mm in the slowly solidified sample and concentrated to 65-69% Si, whilst by 0 mT uniform distribution was observed. In contrast to [30], Zou et al. [46] trying to control behavior of primary Si and the segregation in an Al-30 wt.% Si alloy, observed that for the realization of Si separation, the temperature gradient is a precondition. Secondly, electromagnetic stirring forming a Si-rich layer with 65~70 wt.% Si content, can strengthen the separation effect for Si but is not decisive.

In the present paper shown Si separation by only natural convection, confirms the important role of the temperature gradient found in [45-47], whilst caused by RMF Si reduction seems to result from the Si crystal movement induced by secondary azimuthal flow. The purely eutectic center (Figure 5,7 and 8) contradicts [30] where Si crystals were also observed in the center but agrees with overwhelming results mentioned previously. The reduction of Si crystals observed on Figures 5,7 and 8, may come from liquid flowing throughout the sample and reducing the temperature gradient, that seems to be very important, prerequisite [45-47]. More research should cover the topics of the cooling rate, temperature gradients and the strength of magnetic field.

For Mn-phases, the phenomena of dimension and number density modification seems to be connected also with mechanical interaction, precipitation sequence and with precipitation temperature of phases. Forced convection reducing solutal and thermal diffusion layers, seems to decrease constitutional undercooling through. The reduction of Si crystals seems to be caused by the flow lowering the temperature gradient throughout the sample and the mixing and homogenization of the Si concentration as the Si element moves into the AlSi eutectics, distributed throughout the whole sample. The explanation need more detailed experiments, focused on growth mechanism of Mn-phases.

5. Conclusions

1. The forced flow generated by electromagnetic stirring caused complex modification in microstructure, changed the dimension, amount and location of Mn rich phases and Si crystals, spacing in Al-Si eutectics and shape of α-Al phase, and the observed modifications depend on the alloys composition. In this meaning, the current study helps in understanding of what changes in complex technical alloys may occur,
2. In AlSi12.546Mn1.011 alloy (Mn-first), where $Al_{15}Si_2Mn_4$ precipitate as first and only one till eutectic reaction, for pre-eutectic large Mn-phases, forced convection decreased slightly number density, whilst the overall dimension did not change. The location across sample also stayed unchanged and no movement or separation was observed,
3. In AlSi14.870Mn1.159 alloy (Mn/Si), where $Al_{15}Si_2Mn_4$ precipitate by joint growth together with Si crystal, for pre-eutectic large Mn-phases, forced convection increased the overall dimension and decreased number density. Mn-phases grew in the outside of cylindrical sample,
4. Forced flow strengthened the tendency for growth of pre-eutectic Mn-phases in the outside of cylindrical sample in hypereutectic Mn/Si alloy (AlSi14.870Mn1.159), in opposite to eutectic Mn-first alloy,
5. In the hypereutectic alloys (AlSi14.732Mn0.567 and AlSi16.050Mn0.558), where Si crystals precipitate as the first and only one phase, a great reduction in Si crystals was observed. Flow reduced number density (by 52% and 75%) and moved Si crystals into the thin layer outside the cylindrical sample and also changed average length of Si phases. The reduction in amount of Si crystals seems to be caused by the lower temperature gradient as flow effect, the homogenization and the movement of the Si element to AlSi eutectics,
6. Also by joint growth of Si crystals and Mn-phases, in hypereutectic Mn/Si alloy (AlSi14.870Mn1.159), for Si crystals, forced convection reduced number density by 81%, increased dimension and moved Si into the thin layer outside,
7. The presented common movement of Si crystals and Mn-phases to the outside is completely new and require more investigations. It may open new way for these elements separation, or in control of their content in alloys. It seems also important by metallurgical processes, continuous casting of billets and in the production of Si for the solar photovoltaic industry.

Acknowledgements

The research leading to these results has received partial funding from the People Programme (Marie Curie Actions) of the European Union's Seventh Framework Programme (FP7/2007–2013) under the REA grant agreement n° PCIG13-GA-2013-613906. More information on the funded projects is available at: www.iFlowFePhase.info. This research was partially founded by the Ministry of Science and Higher Education in Poland, allocated at Poznan University of Technology, grant number 0613/SBAD/4770.

References

[1] Mondolfo, L.F. *Aluminium Alloys: Structure and Properties*. London: Butterworths & Co.: UK, 1976.
[2] Nong, G. (Ed.). *Aluminum Alloys*. MDPI. Switzerland, 2018.
[3] Mikolajczak, P. & Ratke, L. (2014). Three Dimensional Morphology of Mn Rich Intermetallics in AlSi Alloys Investigated with X-Ray Tomography. *Materials Science Forum - Solidification and Gravity SolGrav VI*., *Miskolc.* 790-791, 335-340. https://doi.org/10.4028/www.scientific.net/MSF.790-791.335.
[4] Das, A., Ji, S., Fan, Z. (2002). Solidification microstructures obtained by a novel twin screw liquidus casting method. In Proceedings of the 7th International Conference on Demi-Solid Processing of Alloys and Composites,25–27 September 2002 (pp. 689-694). Tsukuba, Japan.
[5] Zhang, Y., Patel, J.B., Lazaro-Nebreda, J. & Fan, Z. (2018). Improved defect control and mechanical property variation in high-pressure die casting of A380 alloy by high shear melt conditioning. *JOM*. 70, 2726-2730. https://doi.org/10.1007/s11837-018-3005-y.
[6] Sree Manu, K.M., Barekar, N.S., Lazaro-Nebreda, Patel, J.B. & Fan, Z. (2021). In-situ microstructural control of A6082 alloy to modify second phase particles by melt conditioned direct chill (MC-DC) casting process – A novel approach. *Journal of Materials Processing Technology*. 295, 117170. https://doi.org/10.1016/j.jmatprotec.2021.117170.
[7] Brollo, G.L., Proni, C.T.W. & Zoqui, E.J. (2018). Thixoforming of an Fe-Rich Al-Si-Cu Alloy—thermodynamic characterization, microstructural evolution, and rheological behavior. *Metals*. 8, 332. https://doi.org/10.3390/met8050332.
[8] Haga T. & Suziki, S. (2001). Casting of aluminum alloy ingots for thixoforming using a cooling slope. *Journal of Materials Processing Technology*. 118(1-2), 169-172. https://doi.org/10.1016/S0924-0136(01)00888-3.
[9] Wang, H., Davidson, C.J. & St. John, D.H. (2004). Semisolid microstructural evolution of AlSi7Mg during partial remelting. *Materials Science and Engineering: A*. 368(1-2), 159-167. https://doi.org/10.1016/j.msea.2003.10.305.
[10] Eslami, M., Payandeh, M., Deflorian, F. & Jarfors, A.E.W., Zanella, C. (2018). Effect of segregation and surface condition on corrosion of Rheo-HPDC Al–Si alloys. *Metals*. 8, 209. https://doi.org/10.3390/met8040209.
[11] Mohammed, M.N., Omar, M.Z., Al-Zubaidi, S., Alhawari, K.S. & Abdelgnei, M.A. (2018). Microstructure and mechanical properties of thixowelded AISI D2 tool steel. *Metals*. 8, 316. https://doi.org/10.3390/met8050316.
[12] Flemings, M. (1991). Behavior of metal alloys in the semisolid state. *Metallurgical Transactions B*. 22B, 269-293. https://doi.org/10.1007/BF02651227.
[13] Modigell, M., Pola, A. & Tocci, M. (2018). Rheological characterization of semi-solid metals: a review. *Metals*. 8, 245. https://doi.org/10.3390/met8040245.

[14] Li, Y., Zhou, R., Li, L., Xiao, H. & Jiang, Y. (2018). Microstructure and properties of semi-solid ZCuSn10P1 alloy processed with an enclosed cooling slope channel. *Metals*. 8, 275. https://doi.org/10.3390/met8040275.
[15] Jiang, J., Xiao, G., Che, C. & Wang, Y. (2018). Microstructure, mechanical properties and wear behavior of the rheoformed 2024 aluminum matrix composite component reinforced by Al_2O nanoparticles. *Metals*. 8, 460. https://doi.org/10.3390/met8060460.
[16] He, M., Zhang, Z., Mao, W., Li, B., Bai, Y. & Xu, J. (2019). Numerical and experimental study on melt treatment for large-volume 7075 alloy by a modified annular electromagnetic stirring. *Materials*. 12, 820. https://doi.org/10.3390/ma12050820.
[17] Nakato, H., Oka, M., Itoyama, S., Urata, M., Kawasaki, T., Hashiguchi, K. & Okano, S. (2002). Continuous semi-solid casting process for aluminum alloy billets. *Materials Transactions*. 43, 24-29. https://doi.org/10.2320/matertrans.43.24.
[18] Mikolajczak, P., Janiszewski, J. & Jackowski, J. (2019). Construction of the facility for aluminium alloys electromagnetic stirring during casting. In Gapiński B., Szostak M., Ivanov V. (Eds.), *Advances in manufacturing II. Vol. 4. Mechanical Engineering* (pp. 164-175). Cham, Switzerland, Springer. https://doi.org/10.1007/978-3-030-16943-5_15.
[19] Mikolajczak, P. (2023). Distribution and Morphology of α-Al, Si and Fe-Rich Phases in Al–Si–Fe Alloys under an Electromagnetic Field. *Materials*. 16, 3304. https://doi.org/10.3390/ma16093304.
[20] Mikolajczak, P. (2017). Microstructural evolution in AlMgSi alloys during solidification under electromagnetic stirring. *Metals*. 7, 89. https://doi.org/10.3390/met7030089.
[21] Mikolajczak, P. (2021). Effect of rotating magnetic field on microstructure in AlCuSi alloys. *Metals*. 11, 1804. https://doi.org/10.3390/met11111804.
[22] Mikolajczak, P. & Ratke, L. (2015). Thermodynamic assessment of mushy zone in directional solidification. *Archives of Foundry Engineering*. 15(4), 101-109. DOI: 10.1515/afe-2015-0088.
[23] Belov, N.A., Aksenov, A.A., Eskin, D.G. (2002). *Iron in Aluminium Alloys—Impurity and Alloying Element*. 1st ed. London, UK: Taylor and Francis Group. https://doi.org/10.1201/9781482265019.
[24] Shabestari, S.G. (2004). The effect of iron and manganese on the formation of intermetallic compounds in aluminum-silicon alloys. *Materials Science and Engineering: A*. 383(2), 289-298. https://doi.org/10.1016/j.msea.2004.06.022.
[25] Thermo-Calc 4.1—Software package from Thermo-Calc Software AB. Stockholm. Sweden. Retrieved June 10, 2023, from www.thermocalc.se.
[26] Fang, X., Shao, G., Liu, Y.Q. & Fan. Z. (2007). Effects of intensive forced melt convection on the mechanical properties of Fe containing Al-Si based alloys. *Materials Science and Engineering: A*. 445-446, 65-72. https://doi.org/10.1016/j.msea.2006.09.038.
[27] Nafisi, S., Emad, D., Shehata, T. & Ghomashchi, R. (2006). Effects of electromagnetic stirring and superheat on the microstructural characteristics of Al-Si-Fe alloy. *Materials Science and Engineering: A*. 432(1-2), 71-83. https://doi.org/10.1016/j.msea.2006.05.076.
[28] Steinbach, S., Euskirchen, N., Witusiewicz, V., Sturz, L. & Ratke, L. (2007). Fluid flow effects on intermetallic phases in Al-cast alloys. *Transactions of Indian Institute of Metals*. 60(2), 137-141. https://doi.org/10.4028/www.scientific.net/MSF.519-521.1795.
[29] Mikolajczak, P. & Ratke, L. (2013). Effect of stirring induced by rotating magnetic field on β-Al5FeSi intermetallic phases during directional solidification in AlSi alloys. *International Journal of Cast Metals Research*. 26, 339-353. https://doi.org/10.1179/1743133613Y.0000000069.
[30] Jie, J.C., Zou, Q.C., Wang, H.W., Sun, J.L. & Lu, Y.P., Wang, T.M., Li, T.J. (2014). Separation and purification of Si from solidification of hypereutectic Al-Si melt under rotating magnetic field. *Journal of Crystal Growth*. 399, 43-48. http://dx.doi.org/10.1016/j.jcrysgro.2014.04.003.
[31] Wenzhou, Y., Wenhui, M., Guoqiang, L., Haiyang, X., Li, S. & Dai, Y. (2014). Effect of electromagnetic stirring on the enrichment of primary silicon from Al-Si melt. *Journal of Crystal Growth*. 405, 23-28. http://dx.doi.org/10.1016/j.jcrysgro.2014.07.035.
[32] Ma, X., Lei, Y., Yoshikawa, T., Zhao, B. & Morita, K. (2015). Effect of solidification conditions on the silicon growth and refining using Si-Sn melt. *Journal of Crystal Growth*. 430, 98-102. http://dx.doi.org/10.1016/j.jcrysgro.2015.08.001.
[33] Zhu, K., Hu, J., Ma, W., Wei, K., Lv, T. & Dai, Y.(2019). Effect of solidification parameters and magnetic field on separation of primary silicon from hypereutectic Ti-85 wt.% Si melt. *Journal of Crystal Growth*. 522, 78-85. https://doi.org/10.1016/j.jcrysgro.2019.05.012.
[34] Li, Y., Liu, L. & Chen, J. (2021). Effect of mechanical stirring on silicon purification during Al-Si solvent refining. *Journal of Crystal Growth*. 553, 125943. https://doi.org/10.1016/j.jcrysgro.2020.125943
[35] Ban, B., Li, Y., Zou, Q., Zhang, T., Chen, J. & Dai, S. (2015). Refining of metallurgical grade Si by solidification of Al-Si melt under electromagnetic stirring. *Journal of Materials Processing Technology*. 222, 142-147. http://dx.doi.org/10.1016/j.jmatprotec.2015.03.012.
[36] Zhang, Y., Miao, X., Shen, Z., Han, Q., Song, C. & Zhai, Q. (2015). Macro segregation formation of the primary silicon phase in directionally solidified Al-Si hypereutectic alloys under the impact of electric currents. *Acta Materialia*. 97, 357-366. http://dx.doi.org/10.1016/j.actamat.2015.07.002.
[37] Li, J., Ni, P., Wang, L. & Tan, Y. (2017). Influence of direct electric current on solidification process of Al-Si alloy. *Materials Science Semiconductor Processing*. 61, 79-84. http://dx.doi.org/10.1016/j.mssp.2016.12.034.
[38] Lv, G., Bao, Y., Zhang, Y., He, Y., Ma, W. & Leu, Y. (2018). Effects of electromagnetic directional solidification conditions on the separation of primary silicon from Al-Si alloy with high Si content. *Materials Science Semiconductor Processing*. 81, 139-148. https://doi.org/10.1016/j.mssp.2018.03.006.
[39] Yoshikawa, T. & Morita, K. (2005). Refining of Si by the solidification of Si-Al melt with electromagnetic force. *ISIJ*

International. 45, 7, 967-971. https://doi.org/10.2355/isijinternational.45.967.

[40] Huang, F., Zhao, L., Liu, L., Hu, Z., Chen, R. & Dong, Z. (2019). Separation and purification of Si from Sn-30Si alloy by electromagnetic semi-continuous directional solidification. *Materials Science in Semiconductor Processing*. 99, 54-61. https://doi.org/10.1016/j.mssp.2019.04.015.

[41] He, Y., Yang, X., Duan, L., Li, S., Chen, Z., Ma, W., Lv, G. & Xing, A. (2021). Silicon separation and purification process from hypereutectic aluminum-silicon for organosilicon use. *Materials Science in Semiconductor Processing*. 121, 105333. https://doi.org/10.1016/j.mssp.2020.105333.

[42] Jiang, W., Yu, W., Li, J., You, Z., Li, C. & Lv, X. (2018). Segregation and morphological evolution of Si phases during electromagnetic directional solidification of hypereutectic Al-Si alloys. *Materials*. 12(1), 10. https://doi.org/10.3390/ma12010010.

[43] Xue, H., Lv, G., Ma, W., Chen, D. & Yu, J. (2015). Separation mechanism of primary silicon from hypereutectic Al-Si melts under alternating electromagnetic fields. *Metallurgical and Materials Transactions A*. 46, 2922-2932. DOI: 10.1007/s11661-015-2889-1.

[44] Li, X., Ren, Z. & Fautrelle, Y. (2009). Effect of a high magnetic field on the distribution of the solute Si and the morphology of the primary Si phase. *Materials Letters*. 63, 1235-1238. doi:10.1016/j.matlet.2009.02.030.

[45] Sun, Jl., Zou, Qc., Jie, Jc. & Li, T. (2016). Separation of primary Si and impurity boron removal from Al-30%Si-10%Sn melt under a traveling magnetic field. *China Foundry*. 13, 4, 284-288. https://doi.org/10.1007/s41230-016-6036-4.

[46] Zou, Q., Tian, H., Zhang, Z., Sun, C., Jie, J., Han, N. & An, X. (2020). Controlling segregation behaviour of primary Si in hypereutectic Al-Si alloy by electromagnetic stirring. *Metals*. 10, 1129. https://doi.org/10.3390/met10091129.

[47] Zou, Q., Han, N., Zhang, Z., Jie, J., Xu, F. & An, X. (2020). Enhancing segregation behaviour of impurity by electromagnetic stirring in the solidification process of Al-30Si alloy. *Metals*. 10, 155. doi:10.3390/met10010155.

[48] Zou, Q., Jie, J., Wang, T. & Li, T. (2016). An efficient method to purify metallurgical grade Si by electromagnetic semi-continuous casting of Al-30Si melt. *Materials Letters*. 185, 59-62. http://dx.doi.org/10.1016/j.matlet.2016.08.103.

[49] Kurz, W., Fisher, D.J. *Fundamentals of Solidification*. Switzerland: Trans Tech Publications.

[50] Dantzig, J.A., Rappaz, M. (2009). *Solidification*. Lausanne, Switzerland: EPFL Press.

[51] Stefanescu, D. (2009). *Science and Engineering of Casting and Solidification*. Boston, MA, USA: Springer. https://doi.org/10.1007/b135947.

[52] Steinbach, S. & Ratke, L. (2007). The influence of fluid flow on the microstructure of directionally solidified AlSi-base alloys. *Metallurgical and Materials Transactions A*. 38, 1388-1394. https://doi.org/10.1007/s11661-007-9162-1.

[53] Martinez, R.A. & Flemings, M.C. (2005). Evolution of particle morphology in semisolid processing. *Metallurgical and Materials Transactions A*. 36, 2205-2210. https://doi.org/10.1007/s11661-005-0339-1.

[54] Niroumand, B. & Xia, K. (2000). 3D study of the structure of primary crystals in a rheocast Al-Cu alloy. *Materials Science and Engineering A*. 283(1-2), 70-75. https://doi.org/10.1016/S0921-5093(00)00619-5.

[55] Birol, Y. (2007). A357 thixoforming feedstock produced by cooling slope casting. *Journal of Materials Processing Technology*. 186(1-3), 94-101. https://doi.org/10.1016/j.jmatprotec.2006.12.021.

[56] Das, A., Ji, S. & Fan, Z. (2002). Morphological development of solidification structures under forced fluid flow: A Monte Carlo simulation. *Acta Materialia*. 50(18), 4571-4585. https://doi.org/10.1016/S1359-6454(02)00305-1.

[57] Li, T., Lin, X. & Huang, W. (2006). Morphological evolution during solidification under stirring. *Acta Materialia*. 54, 4815-4824. https://doi.org/10.1016/j.actamat.2006.06.013.

[58] Mullis, A. (1999). Growth induced dendritic bending and rosette formation during solidification in a shearing flow. *Acta Materialia*. 47, 1783-1789. https://doi.org/10.1016/S1359-6454(99)00052-X.

[59] Marsh, S.P. & Glicksman, M.E. (1996). Overview of geometric effects on coarsening of mushy zones. *Metallurgical and Materials Transactions A*. 27, 557-567. https://doi.org/10.1007/BF02648946.

[60] Loué, W.R. & Suéry, M. (1995). Microstructural evolution during partial remelting of AlSi7Mg alloys. *Materials Science and Engineering A*. 203(1-2), 1-13. https://doi.org/10.1016/0921-5093(95)09861-5.

[61] Mikolajczak, P. & Ratke, L. (2011). Intermetallic phases and microstructure in AlSi alloys influenced by fluid flow. *The Minerals, Metals & Materials Society. TMS*. 10, 9781118062173. https://doi.org/10.1002/9781118062173.ch104.